DRAFT for FNAL Internal Review: Please do not distribute beyond review team

GQuEST: Gravity from the Quantum Entanglement of Spacetime

GQuEST Team

(Dated: September 18, 2023)

The GQuEST experiment uses tabletop-scale Michelson interferometers to sensitively probe for fluctuations in space-time. We present an interferometer design featuring a novel photon counting method to enhance sensitivity. We evaluate its ability to measure space-time fluctuations motivated by quantum gravity models.

I. INTRODUCTION

Quantum gravity research probes the long-standing conundrum of Quantum Mechanics and General Relativity at the Planck scale. The study of quantum gravity is challenged by the vast difference in scale between theoretical observables and direct experimental observations. An international collaboration of theorists, led by KZ, pursues ways to observe signatures of quantum gravity.[1] This work incorporates the entanglement of quantum states on surfaces that define regions of space (*e.g.* [1–3]).

These states are not directly observable. However, an essential conclusion of the theory is accessible to experimental tests: an isotropic, spherical breathing perturbation of the metric described by a scalar field [4] ϕ, by

$$ds^2 = -dt^2 + (1-\phi)(dr^2 + r^2 d\Omega^2). \tag{1}$$

This scalar field represents the degrees of freedom fluctuating from entanglement entropy and the influence of those degrees on gravitation. This field ϕ is predicted to obey wave equations and have a thermal distribution. Metric fluctuations from this scalar field ϕ will be measured (or constrained) by the GQuEST experiment.

Compared to the null case ($\phi = 0$, everywhere), a photon accumulates a change of phase while propagating according to the metric defined in Eq. (1). Consider a Michelson interferometer (IFO), which measures the differential phase of two light beams that have travelled two paths. After sampling the metric of Eq. (1) along different paths, this differential phase carries the observable fluctuation signal.

In Section II A, we discuss the motivation for this fluctuation in the metric from quantum gravity. Several approaches result in similar predictions, encouraging us to bridge the chasm between the Planck scale and observations. In Section II B we describe how IFOs manifest this signal. In Section III we compare the statistics of the standard "fringe readout" of an IFO to a novel "photon counting" method. We present conceptual and reference IFO designs in Section IV.

[1] http://www.qurios.caltech.edu/

II. THEORETICAL MOTIVATION

A. Quantum Gravity Models

A comprehensive review of Quantum Gravity is beyond the scope of this paper. We focus on recent work that predicts observables that are within reach. The "VZ effect" was proposed in Ref. [5], where the quantum nature of gravity implies metric fluctuations which, when integrated over macroscopic distances, yield measurable uncertainties. As these fluctuations of space-time geometry are associated with the quantum degrees of freedom counted by the entanglement entropy, they are referred to as 'geontropic' fluctuations. The status of theoretical work up to the year 2022 is summarized in Ref. [6], showing that diverse theoretical approaches predict metric fluctuations. Ref. [7] describes how shock-wave geometries give rise to these fluctuations. Details of the sensitivity of interferometers to the VZ effect are described in Ref. [4] with several observables: power spectral density, angular correlations, and IR cutoff. Ref. [8] considers future gravitational wave detectors, concluding that the VZ effect could have a significant impact on those missions.

These theories of geontropic fluctuations consistently determine that the scale of total RMS length fluctuations, induced by the metric, is given by

$$\langle \delta L^2 \rangle = \alpha \frac{l_p L}{4\pi} \approx \alpha \left(5.7 \cdot 10^{-18}\mathrm{m}\right)^2 \left(\frac{L}{5\ \mathrm{m}}\right), \tag{2}$$

where we use a convention for the Planck length of $l_p = \sqrt{8\pi\hbar G/c^3}$, and L is the measurement length. For reference, we normalize L to an experimental scale of 5m. Theoretical uncertainty in the fluctuation magnitude is encapsulated in the parameter α. Of particular note is that diverse approaches to quantum gravity yield $\alpha = \mathcal{O}(1)$. These include analyses from conformal field theory [3], dilaton theory [9], and hydrodynamics [10].

B. IFO Signal from Geontropic Fluctuations

An IFO uses laser light at optical frequency ν to measure the phase difference accumulated after traversing two arms. The predicted fluctuations define an auto-correlation

function. This theoretical auto-correlation function of the geontropic fluctuations in the frequency domain, $S_L^\phi(f)$, is the one-sided signal power spectral density (PSD), as a function of frequency f. We express the PSD in terms of the effective displacements corresponding to the measured phase fluctuations in an IFO. We use this signal $S_L^\phi(f)$ to motivate, design, and benchmark experimental tests.

The theoretical PSD is detailed in Ref. [4]. We will use the PSD of the "pixellon" model in this paper, a low-energy (*i.e.* at energies well below the Planck scale) effective description of the full theory, to guide the reference design. Note, however, that a definitive first-principles calculation of the PSD from the fully complete theory is still underway. The pixellon model PSD does not have a concise closed-form expression so the full expression is elided here. Its functional from is depicted in Fig 1, but several specific properties are relevant for calculating experimental requirements. The peak level of the spectral density, $\overline{S}_L^\phi$ is given by [4]:

$$\overline{S}_L^\phi = \alpha \frac{l_p L^2}{c 8\pi^2} \approx \alpha \left(2.9{\cdot}10^{-22} \frac{\mathrm{m}}{\sqrt{\mathrm{Hz}}}\right)^2 \left(\frac{L}{5\ \mathrm{m}}\right)^2. \qquad (3)$$

The signal strength scales with the measurement length as L^2. It also scales with the theoretical uncertainty parameter α, which we seek to measure or bound.

From numerical evaluations of the PSD, we find that the peak of the spectrum is f_{pk} with a signal bandwidth of Δf of:

$$f_{\mathrm{pk}} \approx 15.6\ \mathrm{MHz}\left(\frac{5\ \mathrm{m}}{L}\right), \qquad \Delta f \approx 36\ \mathrm{MHz}\left(\frac{5\ \mathrm{m}}{L}\right), \qquad (4)$$

We use a convention of an over-bar to indicate the peak value or most representative level of a spectrum. For the signal spectrum, this is given by $\overline{S}_L^\phi \equiv S_L^\phi(f_{\mathrm{pk}}) \geq S_L^\phi(f)$. Note from Fig. 1 that the signal is broadband with multiple peaks, and the definition of the signal bandwidth is somewhat arbitrary. The 3db full-width-half-maximum bandwidth, which is approximately 16 MHz, is not suitable here; instead we use $\Delta f \approx 36$ MHz as motivated in the following section.

The amplitude depends on the angle between the two IFO arms. The amplitudes indicated in this work are for $\Theta = 90°$. The amplitude decreases to zero as $\Theta \to 0°$. The precise angular correlation is discussed in [4, 5].

The use of two instruments to detect geontropic fluctuations can be advantageous, as the signal is expected to be correlated for co-located IFOs, and dominant noises are not. Two co-located IFOs have an overlap characterized by the separation between their beamsplitters, s. Following the treatment in [8] the coherence at f_{pk} is 0.88 for $s/L = 0.3$.

III. EXPERIMENTAL APPROACH

A. Laser Interferometry

A Michelson interferometer (IFO) operates by shining light at a beam splitter, which reflects half the power into one arm and transmits the other half into the other arm. The arms are typically 90 degrees apart. The light in each arm then hits an end mirror and is reflected back. The returning light from each arm path is split again as it interacts with the beamsplitter, either returning towards the light source or exiting through the output port. When the IFOs arm lengths are exactly equal, the returning optical fields destructively interfere, returning light towards the source.

If the arms are set to have slightly different lengths, the destructive interference is imperfect and the output port emits a small amount of "fringe" light. Perturbations of the arm lengths then produce modulations of this light level, allowing the difference in arm length to be inferred by continuously monitoring the output light power P_{out}. This readout technique is called "DC readout" or "fringe readout" in the interferometry community, as it uses the constant or DC fringe light as a local oscillator. The use of a local oscillator field from the fringe makes this a form of optical homodyne readout. The method is analogous to homodyne detection in radio and microwave electronic systems.

In practice, arm lengths are subject to low-frequency variations due to environmental effects. P_{out} generates feedback control for the end mirror positions to maintain P_{out} at a set point, typically a small fraction of power incident on the beam splitter. In Fig. 2 these are labeled as "Homodyne Readout" and "Feedback Control." Motions due to temperature variation, mechanical vibration, and other mechanical perturbations manifest on the amplitude of P_{out}. The signal fluctuations also manifest on P_{out}, but at much higher frequencies than most environmental backgrounds.

Any signal that perturbs the optical path length of light traveling inside an interferometer causes a phase modulation of the light. This can equivalently be described as the conversion of input laser light to light with a frequency offset from the source; these new frequency components of the optical field are typically called sidebands. For a modulation (i.e. a signal perturbation) at frequency f, the input laser field at frequency $\nu = c/\lambda$ is modulated to create sideband fields at frequencies $\nu + f$ and $\nu - f$. Those fields beat with the fringe field and modulate the output power P_{out}, which constitutes the IFO's signal. The following sections calculate the quantum limits to resolving such signals, first by using a fringe readout, and second by directly detecting the power in optical light sidebands.

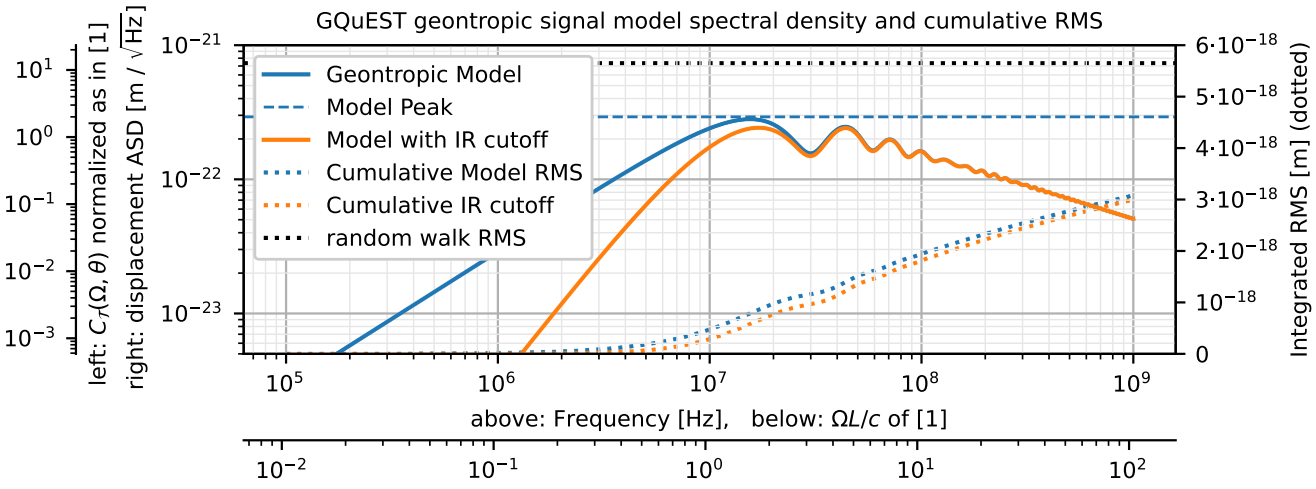

FIG. 1. PSD of the GQuEST geontropic signal. The additional axes show the units of [4].

B. Fringe Readout

The fringe light power P_{out} varies due to photon shot noise [11, 12], which limits the ability to resolve small modulations of P_{out} due to signals. When operating the IFO near destructive interference, i.e. at a dark fringe, the shot noise level does not depend on the choice of fringe power, only on the circulating power on the beamsplitter, P_{BS}. The standard quantum limit from shot noise, $\overline{S}_L^q$, expressed as a one-sided spectral density of the equivalent differential arm length perturbations, is [13, 14]:

$$\overline{S}_L^q = \frac{\hbar c}{2kP_{\text{BS}}} \approx \left(6.2\cdot 10^{-19}\,\frac{\text{m}}{\sqrt{\text{Hz}}}\right)^2 \left(\frac{10\text{kW}}{P_{\text{BS}}}\right)\left(\frac{\lambda}{1.5\mu\text{m}}\right). \quad (5)$$

It applies for any form of homodyne readout of an IFO. We express Eq. (5) using the optical wavelength and power at the beamsplitter from the reference design in Section IV.

This noise level $\overline{S}_L^q$ is only one of many noise contributions; the other noises arise from classical processes that create fluctuations of the IFO arm length or the phase and amplitude of the light. At the signal peak frequency, these classical noises can be engineered to be substantially smaller than the quantum noise $\overline{S}_L^q$. However, the classical noises will not be negligible when photon counting, described in Section III C, is used.

The peak signal level $\overline{S}_L^\phi$ given by Eq. (3) is below the shot noise $\overline{S}_L^q$ given by Eq. (5) by seven orders of magnitude. However, given sufficient measurement time, conventional interferometers using homodyne readout could eventually be able to detect the signal. The geontropic fluctuations $\overline{S}_L^\phi$ manifest as a stochastic noise-like broadband displacement signal, and this can be detected as excess noise on top of the known quantum shot noise. The SNR of a search for excess noise due to geontropic fluctuations in a shot-noise-limited interferometer is given by [14]

$$\text{SNR}^2_{\text{fringe}} = \int_0^T \int_0^\infty \left(\frac{S_L^\phi(f)}{S_L^q(f)}\right)^2 \mathrm{d}f\,\mathrm{d}t \approx T\Delta f \left(\frac{\overline{S}_L^\phi}{\overline{S}_L^q}\right)^2, \quad (6)$$

$$\approx \alpha^2 \left(\frac{T}{160\text{hr}}\right)\left(\frac{10\text{kW}}{P_{\text{BS}}}\right)^2\left(\frac{5\text{ m}}{L}\right). \quad (7)$$

Where T is the total measurement time. Note that our definition of Δf as stated above is chosen to make the approximation of Eq. (6) exact, to account for the specific spectral shape of the signal for fringe readout searches. The time required to create a $\text{SNR}^2 = 9$, or 3σ significance test for $\alpha = 1$ would then be around 2 months of continuous operation.

This suggests that a 5-m IFO using fringe readout is a feasible means to search for this signal, but would require significant measurement time. Additionally, confirming the presence of excess noise due to the diminutive geontropic fluctuations using a single interferometer with homodyne readout requires precise and stable calibrations of the shot noise level, that are difficult to achieve.

C. Photon Counting

The GQuEST experiment will use fringe readout as described above to control IFO arm length difference at low frequencies. However, the main design feature expected to provide GQuEST with its superlative sensitivity is the new, recently proposed technique of single-photon signal sideband readout [14], also called photon counting. The photon counting method involves the elimination of quantum shot noise in the measurement by filtering the output signal of the interferometer, such that single photons carrying the signal of interest can be detected. The elimination of this noise enables the GQuEST IFOs to bypass the quantum shot noise limit, fundamentally beating homodyne

readout, and attaining unprecedented sensitivities within relatively short measurement times.

To explain the advantage of photon counting as proposed for the GQuEST experiment, we start by considering operating an IFO at perfect destructive interference. In this case, there is no fringe light at the output port of the IFO; any light observed at the output implies either the presence of a signal or the presence of some classical noise that perturbs the interferometer arms. If the quantum gravity signal is weak and the classical noise is negligible, one may count single signal photons exiting the output port.

The geontropic length fluctuations produce effective differential interferometer arm length fluctuations $\langle \delta L_{12}^2 \rangle \equiv \langle (\delta L_1 - \delta L_2)^2 \rangle$, where $\delta L_1, \delta L_2$ are the effective length changes of the two individual arms; this is not exactly equal to Eq. (2), as that expression did not yet account for the interferometer antenna response when measuring along two nearby paths simultaneously. A change in the differential arm length produces a proportional change in the flux of photons $\dot{N}$ at the output port, with a constant of proportionality [14]

$$G \equiv \frac{\partial \dot{N}}{\partial \langle \delta L_{12}^2 \rangle} = \frac{k P_{\rm BS}}{\hbar c}, \tag{8}$$

called the optical gain of the interferometer. The differential arm length changes, due to geontropic fluctuations, thus produce a signal photon flux $\dot{N}^\phi$ at the output port given by

$$\dot{N}^\phi = G \langle \delta L_{12}^2 \rangle = \frac{k P_{\rm BS}}{\hbar c} \langle \delta L_{12}^2 \rangle \quad \left(\text{photons} \cdot \text{s}^{-1} = \text{Hz} \right). \tag{9}$$

This total signal photon flux cannot yet be evaluated unequivocally, as the PSD of the pixellon ϕ signal falls off as $1/f$ (see fig. 1), and therefore its integral diverges logarithmically; this can be attributed to the lack of a high-frequency (UV) cut-off in the pixellon theory. We can however evaluate the total photon flux of the signal within some finite detection bandwidth, by integrating over the photon flux spectral density

$$\mathcal{S}_{\dot{N}}^\phi(\epsilon) = G \frac{S_L^\phi(f)}{2} = \frac{S_L^\phi}{4 S_L^q} \quad \text{for } \epsilon = \pm f; \tag{10}$$

this quantity represents the frequency decomposition of the signal sideband photon flux as a *two-sided* spectral density. We use the two-sided spectral density to evaluate the photon flux, as geontropic signals of frequency f produce both lower and upper signal sidebands at optical frequencies $\nu - f$ and $\nu + f$, respectively, that can be separately measured. For this reason, we specifically use ϵ to denote measurements at an optical frequency shift $\epsilon \in [-\nu, \infty]$, to distinguish it from measurements at signal frequency $f \in [0, \infty]$. The last equality in Eq. (10) is obtained from relating the optical gain to the shot noise level as $S_L^q = \frac{1}{2} \cdot G^{-1}$, which expresses that the vacuum state of the electromagnetic field (with an expectation value of $\frac{1}{2}$ quanta) produces spurious displacement signals S_L^q in the output of the interferometer.

To give an impression of the effectiveness of photon counting, we evaluate the signal photon flux due to geontropic fluctuations in a range of frequencies up to Δf above and below the laser source frequency:

$$\dot{N}_{\rm peak}^\phi = \int_{-\Delta f}^{\Delta f} \mathcal{S}_{\dot{N}}^\phi(\epsilon) d\epsilon = \mathcal{O}(1)\,\text{Hz}. \tag{11}$$

For a measurement where photons are counted over an interval dt, the number of accumulated signal photons is $dN = \dot{N} dt$. The variance of the number of accumulated photons is determined by Poisson statistics, $\sigma_{dN}^2 = dN$. Thus, when counting signal photons in an IFO operated at perfect destructive interference without any classical noise, the SNR accumulates over time as

$$\text{SNR}_{\rm count}^2 = \int_0^T \frac{(dN_{\rm peak}^\phi)^2}{dN_{\rm peak}^\phi} \approx T \Delta f \frac{\overline{S}_L^\phi}{2 S_L^q}, \tag{12}$$

$$\approx \alpha \left(\frac{T}{0.25\text{s}} \right) \left(\frac{10\text{kW}}{P_{\rm BS}} \right) \left(\frac{5\text{ m}}{L} \right), \tag{13}$$

where we approximate the spectrum as a constant equal to the peak value over the bandwidth of the signal. This must be approximated given our definition of Δf using a different readout scheme, due to the different power of S_L^ϕ in the integrands of Eqs. (6) and (12). Comparing these two equations indicates that reading the interferometer by counting individual signal-carrying photons is fundamentally and profoundly more efficient than the traditional fringe readout. Under ideal conditions, it requires less than a second to detect geontropic fluctuations with $\alpha = 1$ at 1σ significance, and even a 3σ to 5σ test of the theory would take less than a minute.

In practice, this sensitivity cannot be achieved with current technology, as a realistic interferometer cannot be operated at perfect destructive interference for many reasons. There will always be small amounts of light at the output port of the interferometer due to imperfections in the optics and low frequency length perturbations of the arms. These small amounts of light constitute a photon flux many orders of magnitude greater than the signal in Eq. (9) and would obscure it.

However, the condition of having no static (DC) fringe light at the output port can be emulated by filtering the fringe light, removing all the unwanted optical power. This is done by making use that the output optical field carrying the signal (the signal sideband) has a different frequency than the optical field from both the input laser and much of the classical noise. GQuEST will use optical cavities to strongly filter the output light, letting through only photons with frequencies corresponding to the desired signal. Specifically we model the effect of the cavities as a filter functon $Q(\epsilon) \leq 1$ which is roughly Lorentzian, where $Q(0\,\text{Hz}) \ll 10^{-15}$, $Q(+f_{\rm pk}) \approx 1$, and the FWHM $\Delta\epsilon \approx 25$ kHz.

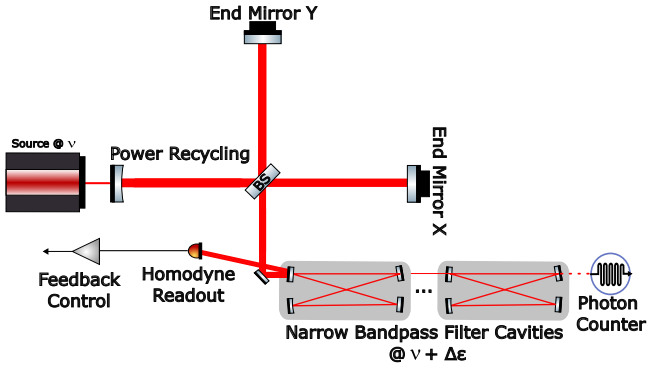

FIG. 2. Simplified sketch of experimental arrangement for one IFO. 1550nm light is incident on a power recycled IFO. The output of the IFO is filtered through narrow bandpass filter cavities, reaching > 200db of isolation with four cavities. The promptly reflected light on the first bandpass filter is used in a homodyne readout scheme to control feedback systems of the IFO.

The filtered photon flux is then

$$\dot{N}^{\phi}_{\rm pass} = \int_{-\nu}^{\infty} \mathcal{S}^{\phi}_{\dot{N}}(\epsilon')Q(\epsilon')d\epsilon' = \int_{\epsilon-\Delta\epsilon/2}^{\epsilon+\Delta\epsilon/2} \mathcal{S}^{\phi}_{\dot{N}}(\epsilon')d\epsilon' \tag{14}$$

$$\approx \frac{\Delta\epsilon \overline{S}^{\phi}_{L}}{4S^{q}_{L}} \approx 10^{-3}\ \text{Hz}, \tag{15}$$

where we neglect the presence of background noise contributions. Below, we expand on the design of the filter cavities to enable photon counting readout. In addition, we proceed to estimate the SNR for the full GQuEST design in the presence of classical noise in the filter passband.

IV. EXPERIMENTAL DESIGN

A. Interferometer Design

Our goal is to build interferometers with a sensitivity that allows the geontropic fluctuations to be measured in a reasonable time. This requires the use of high-power interferometers using photon counting readout. The interferometer diagram in Fig. 2 indicates the essential elements of the design.

The IFO arm length is chosen to be 5 meters, which balances the increase of the signal strength for longer arms with technical constraints on photon counting that favor having the peak of the signal spectrum at higher frequencies (note $f_{\rm pk} \propto 1/L$, Eq. (4)), as discussed in Section IV C. We set the IFO arm angle $\Theta = 90°$ for simplicity. Changing Θ or L modulates the signal strength, and we will modulate L for initial experiments.

The optical power on the beamsplitter will be 10 kW; this represents a compromise between increasing the optical gain of the signal (Eq. (8)), limiting thermal distortion of the optics and reasonably limits of laser power and scattering losses. We use a laser wavelength of $\lambda = 1.5\mu$m to take advantage of the continuing development of optics for this wavelength for future gravitational wave detectors [15], and to minimize thermal distortion of the optics using Silicon substrates.

The interferometer is operated for destructive interference, allowing only a small fraction of the total power on the beamsplitter to be directed down towards the detectors. The remainder returns towards the input laser, where a power-recycling mirror is added to form a resonant cavity between the laser and the beamsplitter. This power-recycling cavity enhances the input laser power of 10 W in the interferometer to 10 kW or more of circulating light. The high operating power can cause thermal distortions of the beamsplitter and mirrors, driving the design choices of the materials and wavelength in the reference design below.

The output light power $P_{\rm out}$ will be on the order of tens of mW, which is small compared to the power on the beamsplitter, but large compared to the expected photon flux due to the geontropic signal.

We use a series of narrowband optical filter cavities at the interferometer output that transmit light at a frequency $\nu + \epsilon$ (where ν is the frequency of the input laser and ϵ is the frequency of the signal). Based on the PSD in II A, we choose a filter cavity offset frequency of $\epsilon = \epsilon_{\rm pk} = 15.6$ MHz, with a filter FWHM bandwidth of 50 kHz. The filters have sufficiently rapid roll-off to suppress photons at a frequency ν. With multiple filters in series, the effective pass bandwidth is $\Delta\epsilon \approx 25$kHz. During operation, the value of ϵ can be varied in the range from 8 to 40 MHz, allowing the frequency dependence of the signal PSD to be resolved, and for diagnostics of the mirror thermal spectrum.

Photons will be detected with single-photon detectors downstream of the filter cavities. We aim to achieve dark count rates for our photo detectors equal to the signal count rate, as the dark count rate will then be negligible compared to the classical noise count rate (see below). Photodetector dark count rates on the order of 10^{-5} Hz are achievable with current technology, specifically with superconducting nanowire single-photon detectors.

Another important part of the IFO design is the implementation of feedback control to maintain the IFO at the operating point. This requires the use of fringe readout to measure low-frequency environmental perturbations. This is implemented using the residual fringe light power at the output $P_{\rm out}$ that is reflected from the first of the filter cavities. The reflected light contains information from the environmental perturbations of the interferometer arms, which can be read out and used to effect feedback control. This readout is ideally done with the balanced-homodyne scheme to minimize the fringe light required to detect the length perturbation; alternatively, the DC (fringe) readout method can be used.

In addition to suppressing light at the main laser frequency, the filter cavities are designed to suppress noise from thermally excited bulk acoustic wave (BAW) modes of the interferometer optics. For thin, disc-like mirrors,

the BAW modes create a spectrum of noise peaks that are regularly and widely spaced across the signal band[16]. The cavity design is chosen such that the filter passband can be chosen to lie between two successive bulk acoustic resonances. Between these spectral lines, there is some broadband thermal noise, which is due both to the tails of the BAW resonances and the thermal fluctuations in the optical coatings. Modelling has been performed to estimate the total thermal noise in the passband of the filter cavities (see below), and it is expected that the total classical thermal noises are on the order of $\overline{S}_L^c \approx \left(10^{-21}\mathrm{m}/\sqrt{\mathrm{Hz}}\right)^2$, which is dominated by coating thermal noise.

Notably, this classical noise level is expected to be slightly above the signal level, which implies a nonzero background photon count rate. Therefore, the sensitivity of the experiment will be limited both by the low flux of signal photons and by the variance of the flux of photons from thermal noise. The statistical impact and experimental remedy are described below.

The fiducial design parameters for the GQuEST IFOs are summarized in Table I.

TABLE I. Parameters of the fiducial IFO design. The noise spectral densities are evaluated at 16 MHz

parameter	symbol	value
Geontropic fluct. scale parameter	α	$\mathcal{O}(1)$
IFO arm length	L	5 m
Power on beamsplitter	P_{BS}	10 kW
Laser wavelength	λ	1.5 μm
Laser frequency	ν	193.4 THz
Nominal filter offset frequency	ϵ	15.6 MHz
Filter bandwidth (FWHM)	$\Delta\epsilon$	25 kHz
Carrier leakage filter limit	ϵ_{min}	8 MHz
Higher-order mode leakage filter limit	ϵ_{max}	40 MHz
Twin IFO separation	s	1.5 m
IFO inter-arm angle	Θ	90°
Signal Spectral Density (peak)	$\overline{S}_L^{\phi}$	$\left(3\cdot10^{-22}\mathrm{m}/\sqrt{\mathrm{Hz}}\right)^2$
Thermal Noise Spectral Density	$\overline{S}_L^{c}$	$\left(10^{-21}\mathrm{m}/\sqrt{\mathrm{Hz}}\right)^2$
Shot Noise Spectral Density	S_L^{q}	$\left(6\cdot10^{-19}\mathrm{m}/\sqrt{\mathrm{Hz}}\right)^2$
Photon Detector Dark Count Rate	$\dot{N}^d$	10^{-3} Hz
Observation time for 5σ test	T	$\mathcal{O}(100)$ hours

B. Operating Modes

1. Single Interferometer

We will initially operate a single IFO with $L < 5$ m to test the design and to commission and characterize all subsystems. We will then extend the arms of the interferometer, which increases the magnitude of the signal from geontropic fluctuations to a detectable level. This configuration will allow the GQuEST experiment to provide a significant detection of a quantum gravity signal using a single interferometer.

This signal would take the form of a measured photon count rate greater than the expected classical noise. The detection could then be investigated further to confirm the origin of the signal as geontropic fluctuations. Specifically, the spectral shape of the signal can be measured by varying the filter offset frequency ϵ. In addition, the dependence of the amplitude of the signal on the arm length of the IFO can be verified by changing the arm length. In future, we could also vary the inter-arm angle Θ to verify the dependence of the signal on this parameter.

2. Two Interferometers

A more reliable confirmation of the presence of a geontropic signal could be obtained with the simultaneous operation of multiple identical GQuEST IFOs placed close together. The expected cross spectral density (CSD) of the signal from geontropic fluctuations in co-located and aligned twin IFOs is expected to be roughly equal to the auto-spectral density in each individual IFO, but with a magnitude reduced by $\approx 10\%$ due to the loss of coherence from the nonzero separation between the IFOs. Thermal noise from the optics is expected to be dominant, and this noise is uncorrelated between different interferometers. As the signal is thus largely correlated between co-located IFOs and the noise is not, the geontropic signal can be identified with two IFOs as a correlated photon flux. Observation of such a correlated signal provides stronger evidence than the observation of a signal in a single IFO, as the former is less likely to be spurious.

C. Reference Sensitivity

To make a realistic estimate of the sensitivity of the interferometers, we have to evaluate the signal count rate, $\dot{N}^{\phi}_{\mathrm{pass}}$, the count rate from classical interferometer noise, $\dot{N}^{c}_{\mathrm{pass}}$ and the dark count rate of the photo detector, $\dot{N}^d$.

The filtered photon flux from classical noise is computed similarly to the computation of the filtered signal photon flux (see Eq. (10) and Eq. (14)), where we substitute S_L^{ϕ} for the classical displacement spectral density S_L^c. In addition, for both the signal and the noise, we model the frequency dependence of the transmission of the optical filter cavities as a filter function $Q(\epsilon)$. The filtered classical noise photon flux is then

$$\dot{N}^c_{\mathrm{pass}} = \int_{-\infty}^{\infty} \mathcal{S}^c_{\dot{N}}(\epsilon) Q(\epsilon) \mathrm{d}\epsilon. \approx \frac{\Delta\epsilon \overline{S}_L^c}{4 S_L^q} \approx 1.6\cdot10^{-2}\,\mathrm{Hz}. \quad (16)$$

The SNR can then bound by considering that the signal accumulates as $\int \mathrm{d}t \dot{N}^{\phi}$, while the total variance is the quadrature sum of all noise count rate contributions, i.e. $\sigma^2_{dN} = \Sigma_i \sigma^2_{dN^i}$, integrated over time. This leads to an SNR

of

$$\mathrm{SNR}^2_{\mathrm{counting}} = \int_0^T \frac{\left(\dot{N}^{\phi}_{\mathrm{pass}}\mathrm{d}t\right)^2}{\left(\dot{N}^{\phi}_{\mathrm{pass}} + \dot{N}^{c}_{\mathrm{pass}} + \dot{N}^{d}\right)\mathrm{d}t}. \tag{17}$$

This can be evaluated as

$$\mathrm{SNR}^2_{\mathrm{counting}} \approx \frac{T\Delta\epsilon}{4}\frac{\overline{S}^{\phi}_L}{S^q_L}\left(1 + \frac{\overline{S}^{c}_L}{S^{\phi}_L} + \frac{4\dot{N}^d}{\Delta\epsilon}\frac{\overline{S}^{q}_L}{\overline{S}^{\phi}_L}\right)^{-1}. \tag{18}$$

Assuming the dark count rate and classical noise are negligible, we estimate the SNR as

$$\mathrm{SNR}^2_{\mathrm{counting}} \approx \frac{T\Delta\epsilon}{4}\frac{\overline{S}^{\phi}_L}{S^q_L} \approx \alpha\left(\frac{T}{12\,\mathrm{min}}\right)\left(\frac{10\mathrm{kW}}{P_{\mathrm{BS}}}\right)\left(\frac{5\ \mathrm{m}}{L}\right)^2. \tag{19}$$

Instead, if we realistically assume that the classical noise is not negligible and is larger than the expected signal level, and in addition we assume the dark count rate is negligible compared to the classical noise, the SNR is given by

$$\mathrm{SNR}^2_{\mathrm{counting}} \approx \frac{T\Delta\epsilon}{4}\frac{\left(\overline{S}^{\phi}_L\right)^2}{S^q_L\overline{S}^{c}_L} \tag{20}$$

$$\approx \alpha^2\left(\frac{T}{2.4\,\mathrm{hr}}\right)\left(\frac{10\mathrm{kW}}{P_{\mathrm{BS}}}\right)\left(\frac{5\ \mathrm{m}}{L}\right)^4\left(\frac{S^c_L(f)}{\overline{S}^{c}_L}\right), \tag{21}$$

where we use a classical noise level $\overline{S}^{c}_L = (10^{-21}\mathrm{m}/\sqrt{\mathrm{Hz}})^2$, which is the expected order of magnitude of the thermal noise (see below).

Thus, two major ways to increase the sensitivity and decrease the required measurement time are to reduce the classical noise and to increase the arm length. Increasing the arm length has the effect of shifting the peak signal frequency to lower frequencies (see Eq. (4)). Importantly, at lower frequencies, the dominant classical noises will be stronger, as the coating thermal noise and substrate thermal noise scale as $1/f$. Additionally, a subdominant noise source might become of influence at lower frequencies; thermorefractive and charge carrier noises have a $1/f^2$ frequency dependence. For this reason, a design with 5-m arms is chosen as an optimum that balances the signal magnitude and classical noise levels at the signal peak.

[1] T. Jacobson, Phys. Rev. Lett. **116**, 201101 (2016), arXiv:1505.04753 [gr-qc].
[2] H. Casini, M. Huerta, and R. C. Myers, JHEP **05**, 036, arXiv:1102.0440 [hep-th].
[3] T. Banks and K. M. Zurek, Phys. Rev. D **104**, 126026 (2021), arXiv:2108.04806 [hep-th].
[4] D. Li, V. S. H. Lee, Y. Chen, and K. M. Zurek, Phys. Rev. D **107**, 024002 (2023).
[5] E. P. Verlinde and K. M. Zurek, Physics Letters B **822**, 136663 (2021).
[6] K. M. Zurek, arXiv e-prints (2022), arXiv:2205.01799 [gr-qc].
[7] E. Verlinde and K. M. Zurek, Phys. Rev. D **106**, 106011 (2022), arXiv:2208.01059 [hep-th].
[8] M. W. Bub, Y. Chen, Y. Du, D. Li, Y. Zhang, and K. M. Zurek, arXiv e-prints , arXiv:2305.11224 (2023), arXiv:2305.11224 [gr-qc].
[9] S. Gukov, V. S. H. Lee, and K. M. Zurek, Phys. Rev. D **107**, 016004 (2023), arXiv:2205.02233 [hep-th].
[10] Y. Zhang and K. M. Zurek, (2023), arXiv:2304.12349 [hep-th].
[11] W. Schottky, Annalen der Physik **362**, 541 (1918).
[12] W. Schottky, M. Burkards, and A. Yesn, Journal of Micro/Nanolithography, MEMS, and MOEMS **17**, 041001 (2018).
[13] C. M. Caves, Phys. Rev. D **23**, 1693 (1981).
[14] L. McCuller, arXiv preprint arXiv:2211.04016 (2022).
[15] F. Meylahn and B. Willke, Instruments **6**, 10.3390/instruments6010015 (2022).
[16] A. Chou, H. Glass, H. R. Gustafson, C. Hogan, B. L. Kamai, O. Kwon, R. Lanza, L. McCuller, S. S. Meyer, J. Richardson, C. Stoughton, R. Tomlin, and R. Weiss, Class. Quantum Grav. **34**, 065005 (2017).